EFFECTS OF SMALL DEFECTS AND INHOMOGENEITIES ON FATIGUE STRENGTH: EXPERIMENTS, MODEL AND APPLICATIONS TO INDUSTRY

Y. Murakami*

Quantitative evaluation method of fatigue strength based on *the √area parameter model* is explained and some applications to industry are introduced. First, the basic concept of *the √area parameter model* is explained based on the experimental evidences that small cracks, defects and nonmetallic inclusions having the same value of the square root of projection area, $\sqrt{area}$, have the identical influence on the fatigue strength regardless of different stress concentration factors. Second, various applications of *the √area parameter model* to various defects by the author's group and Japanese industries are introduced. Finally, other related problems such as the quality control of materials from viewpoint of *the inclusion or defect rating by statistics of extreme* and the effect of small defects on fatigue lives are also discussed.

INTRODUCTION

Experimental studies (1,2) have shown that the value of ΔK_{th} is dependent on the crack size, i.e. the smaller the crack, the smaller the value of ΔK_{th}. Figure 1 shows the values of ΔK_{th} of various materials as the function of crack size; $\sqrt{area}$ (3).

The fact that ΔK_{th} is not a material constant for small cracks must be absolutely considered in fatigue limit prediction and fatigue crack growth prediction. In the present paper, the author discusses the method of fatigue limit prediction by *the √area parameter model* for materials containing small cracks, defects and other inhomogeneities which exist quite commonly in industrial materials.

BACKGROUND OF THE √area PARAMETER MODEL

What is Fatigue Limit ?

The fatigue limit of most materials is not the critical stress for crack initiation but the threshold stress for nonpropagation of the crack which emanated from original cracks, defects or inhomogeneities. There are sufficient experimental

----

Dept. of Mechanical Science and Engineering, Kyushu University, Fukuoka, Higashi-ku, 812-81 Japan

evidences which support this viewpoint. Figure 2 shows an example of such nonpropagating cracks (4). Figure 3 illustrates cracks emanating from an artificial hole and afterward stopped propagating at the fatigue limit (5). This crack is a so-called nonpropagating crack.

When 12 holes with 40μm diameter were introduced on the surface of one specimen at the fatigue limit stress (5), some holes had two nonpropagating cracks at the points of stress concentration of the hole but other holes had only one or no nonpropagating crack (see Fig.3). At the stress 5MPa higher than the fatigue limit, all specimens failed and all specimens had no crack at the stress 5MPa lower than the fatigue limit. Thus, if the microstructure of materials is well controlled, fatigue limit is a phenomenon observed only in narrow band of applied stress[note]. In terms of this viewpoint, the scatter of fatigue strength of high strength steels should not attributed to their hard microstructures, because it is mostly caused by nonmetallic inclusions and not by the microstructure itself. The scatter must be viewed from the influence of nonmetallic inclusions contained in the hard microstructures.

Basic Model

Recognizing the fatigue limit as the threshold of crack propagation is crucially important to make a fatigue limit prediction model. Looking at Fig.1, we notice that ΔK_{th} has a good correlation with $\sqrt{area}$ of defects. The most appropriate geometrical parameter $\sqrt{area}$ was found from the three dimensional crack analysis (6) which shows a strong correlation between K_{Imax} along crack front and $\sqrt{area}$ of crack. Thus, we obtain the following relationship.

$$\Delta K_{th} \propto (\sqrt{area})^{1/3} \tag{1}$$

Looking at Fig.1 again, we notice that the data lines of ΔK_{th} for 15 materials are ordered from lower to higher values depending exactly on the values of their Vickers hardness HV. Thus, applying the least square method to all the data, we have

$$\Delta K_{th} = 3.3 \times 10^{-3} (HV + 120) (\sqrt{area})^{1/3} \tag{2}$$

Rewriting Eq.(2) for fatigue limit stress, we have

$$\sigma_{w0} = 1.43 (HV + 120) / (\sqrt{area})^{1/6} \tag{3}$$

Where, the units are ΔK_{th} :MPa$\cdot$m$^{1/2}$, σ_{w0}:MPa, HV :kgf/mm^2, $\sqrt{area}$:μm.

[note] If we define the fatigue limit by the threshold stress intensity factor range ΔK_{th} using the original defect size $\sqrt{area}$, we can have its definite value depending on the size ($\sqrt{area}$). On the contrary, however if we define the fatigue threshold by the final condition of 12 holes, we have 12 different values of ΔK_{th} for one specimen which produce troubles in fatigue limit prediction. This is the reason why the initial defect size is used in the fatigue limit prediction based on *the $\sqrt{area}$ parameter model*.

In recent studies, Murakami *et al.* extended Eq.(3) to more general cases including R ratio ($R = \sigma_{min} / \sigma_{max}$) as follows.

$$\sigma_w = 1.43 \, (HV + 120) \, / \, (\sqrt{area}\,)^{1/6} \cdot [\, (1 - R) \, / \, 2 \,]^{\alpha} \qquad (4)$$
; for surface defects and inclusions

$$\sigma_w = 1.56 \, (HV + 120) \, / \, (\sqrt{area}\,)^{1/6} \cdot [\, (1 - R) \, / \, 2 \,]^{\alpha} \qquad (5)$$
; for internal defects and inclusions

where,

$$\alpha = 0.226 + HV \times 10^{-4} \qquad (6)$$
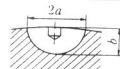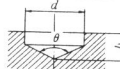
APPLICATIONS OF *THE $\sqrt{area}$ PARAMETER MODEL* TO ARTIFICIAL DEFECTS

Holes and Cracks

From the viewpoint of examining *the $\sqrt{area}$ parameter model*, the comparison of fatigue limit of specimens containing an artificial drilled hole and an artificial surface crack having the identical value of $\sqrt{area}$ is interesting. Table 1 shows the shape of the initial hole and crack (7). The initial crack was introduced by fatigue test using a specimen containing a smaller artificial hole with the diameter of $40\mu m$. The specimen was annealed after preliminary fatigue test to relieve the prior fatigue history. As shown in Table 1, the fatigue limits measured with these two kinds of specimens are completely the same regardless of the big difference in stress concentration factor of hole and crack. Figure 4 shows similar additional fatigue test results which are in good agreement with the predictions reported in Ref.(7).

To examine more in detail the validity of *the $\sqrt{area}$ parameter model*, specimens of a hard steel (maraging steel:HV=510) were tested by tension-compression fatigue (8). As shown in Fig.5, the fatigue limits of the specimen having an initial crack ▲ and a two-hole defect ■ with fatigue crack introduced by preliminary fatigue test are the same (402MPa) for the same value of $\sqrt{area}$, though that for the specimen containing one hole ● is 421MPa which is only 4.7% higher than ■ and ▲.

TABLE 1 – Comparison of rotating bending fatigue limit of specimens containing a small artificial hole and that of specimens containing a small crack (Annealed 0.46% C steel) (7).

Shape of initial hole and crack	$\sqrt{area}$ μm	Experimental value of fatigue limit, σ_w MPa
$2a = 213\mu m$ Aspect ratio: $b/a = 0.7$	112	200.9
$d = 200\mu m$ $h = 100\mu m$ $\theta = 120^{\circ}$	115	200.9

APPLICATIONS TO NONMETALLIC INCLUSIONS

Nonmetallic Inclusions at Fracture Origin

It is quite common that a white circular mark named *fish-eye* is observed on the fatigue fracture surface of high-strength steels. Usually a nonmetallic inclusion exists at the center of a fish-eye. Figure 6 shows the typical nonmetallic inclusion at fish-eye (9). The fatigue fracture origin of high-strength steels is mostly at nonmetallic inclusions such as MnS, Al_2O_3, SiO_2 and TiN having various shapes and sizes. In terms of fatigue limit, we can consider nonmetallic inclusions to be mechanically equivalent to stress-free defects (7).

When nonmetallic inclusions cause fatigue failure, it is very difficult to predict the fatigue strength in advance of fatigue test. We can identify the size and location of the fatal inclusion appeared on the fracture surface of specimen after fatigue fracture. In such cases, the stress applied at the fatal inclusion should be larger than the value which is calculated by the fatigue strength prediction Eq.(4) or (5). Table 2 shows the comparison between such experimental results on a bearing steel and the calculated values (10). We can see that the stresses (σ') applied at the fatal inclusions are actually larger than the estimated fatigue limits (σ_w').

Shape of Inclusions

The experimental facts on holes and cracks shown in Table 1 and Fig.5 suggest that there should be no difference in the influence of inclusion shape if the values of $\sqrt{area}$ of two inclusions are the same. This prediction is completely agreement with the results of the fatigue tests conducted by W. E. Duckworth and E. Ineson (11) who artificially introduced spherical and angular alumina particles into ingots and found no definite difference of effect of inclusion shape. Their experimental data were also arranged successfully by *the $\sqrt{area}$ parameter model* (12).

TABLE 2 – Size and location of inclusions and fatigue limit predicted by Eq.(5)(Rotating bending fatigue, Bearing steel ; HV = 685) (10).

Nominal stress at surface, σ (MPa)	Cycles to failure, N_f	Inclusion size, $\sqrt{area}$ (μm)	Distance from surface, h (μm)	Shape of inclusions	Nominal stress at inclusion, σ' (MPa)	Fatigue limit predicted by Eq.(5), σ_w' (MPa)	σ'/σ_w'
981	50.11×10^4	37.5	80		961	686	1.40
981	39.21	29.3	170		941	715	1.32
932	683.38	32.5	570		807	703	1.15
883	138.24	53.5	200		841	647	1.30
981	75.06	31.0	350		900	708	1.27
932	160.35	25.6	240		878	732	1.20
932	11.12	47.0	100		909	661	1.38
932	23.40	100.7	1030		706	582	1.21
834	420.00	69.9	600		715	619	1.16

In terms of chemical composition and shape of inclusions, the experiments by Monot *et al.* are also interesting. The author received the detailed data from Monot and could rearrange their data successfully by *the √area parameter model* (7). Figure 7 shows the effect of nonmetallic inclusions on fatigue strength of bearing steels.

Controlling the chemical composition of inclusions of spring steels, Murakami *et al.* (9) prepared specimens containing soft and hard inclusions with various shapes. They demonstrated that the size of inclusions is the most crucial factor for fatigue limit regardless of various hardness and shapes of inclusions.

Prediction of Scatter of Fatigue Strength due to Nonmetallic Inclusions

Murakami *et al.* (10,13) proposed a method of predicting the upper and the lower bound of fatigue strength. The upper bound of fatigue strength (The ideal fatigue strength of the microstructure) is obtained when fatigue fracture is not affected by defects or inclusions, and the value can be empirically estimated by Eq.(7).

$$\sigma_{w0} = 1.6HV \pm 0.1HV \quad (HV < 400) \tag{7}$$

The lower bound σ_{wl} of fatigue strength can be obtained when the largest inclusion is located in contact with the surface of a specimen. The prediction equation for σ_{wl} is given by Eq.(8) for the case of R = -1 (13).

$$\sigma_w = 1.41\,(HV + 120) / (\sqrt{area}_{max})^{1/6} \tag{8}$$

where $\sqrt{area}_{max}$ is the expected maximum size of inclusions contained in a definite volume. In order to estimate the expected maximum size of inclusions contained in a definite number of specimens, Murakami *et al.* (7, 14, 15) applied *the method of the statistics of extreme* (16) to the distribution of inclusions. Figure 8 shows the distribution of the maximum size $\sqrt{area}_{max}$ of inclusions observed in the unit area S_0 (= 0.0309mm^2) of two spring steels (Japanese Industrial Standard SAE9254). Estimating the return period T for N specimens, the expected maximum size of inclusion $\sqrt{area}_{max}$ can be determined by the procedure indicated in the figure.

Introducing HV and $\sqrt{area}_{max}$ to Eq.(8), the lower bound σ_{wl} of fatigue strength for N specimens is predicted as in Fig.9. The lower bound of experimental data is well predicted by the equation.

APPLICATIONS TO CAST DEFECTS AND OTHER MATERIAL DEFECTS

Spheroidal Graphites in Cast Irons

Nodular cast iron contains numerous small defects as graphite nodules in the structure (see Fig.10). Since the fatigue strength is strongly affected by the nodules or casting defects, a lot of attempts have been recently made to apply *the √area parameter model* to the fatigue strength evaluation of this material.

TABLE 3 – <u>Comparison of rotating bending fatigue limits predicted from the maximum graphite nodule sizes and the experimental values (17).</u>

Material	$\sqrt{area}_{max}$ (μm)	$\sigma_{w0, pred}$ (MPa)	$\sigma_{w0, exp}$ (MPa)
FCD400	101	202	. 220
FCD700	94	274	280

Figure 10 shows the distribution of nodule size ($\sqrt{area}$) of the material used in the fatigue test by Endo (17). Table 3 demonstrates a good agreement between the experimental results and the prediction by *the $\sqrt{area}$ parameter model*.

When the size ($\sqrt{area}$) of other defects is larger than that of graphite nodules, the fatigue limit of plain specimens is predominantly determined by the defect with the maximum size (18).

Pores in Cast Aluminum Alloy

It is well known that pores contained in cast aluminum alloys cause the low fatigue strength and scatter of fatigue strength.

Kobayashi and Matsui (19) confirmed first the availability of *the $\sqrt{area}$ parameter model* to an aluminum alloy (JIS-AC4C, ASTM356.0) and then applied the same method to the strength design of automobile rocher arm. Figure 11(a) shows the size distribution of pores in the Al alloy. Figure 11(b) shows the S-N curve of the rocher arm with the predicted lower bound of the fatigue limit for 100 parts.

Second Phases in Al-Si Eutectic Alloy

The inhomogeneity phase such as Si in Al-Si eutectic alloys behaves like hard nonmetallic inclusions in fatigue, because the hardness of Si phases is much higher than aluminum matrix. Figure 12 shows a Si-phase observed at the fatigue fracture origin of Al-Si eutectic alloy. The same concept of fatigue strength prediction for nonmetallic inclusions has been successfully applied to this kind of material (20).

Carbides in Tool Steel

Natsume, Muramatsu and Miyamoto (21) conducted interesting experiments on the influence of carbides contained in a tool steel. They prepared specimens containing uncracked carbides by high temperature forming and those containing cracked carbides by room temperature forming. Figure 13(a) shows uncracked carbides and Fig.13(b) shows carbides cracked by room temperature forming. The hardness of the matrix is adjusted to be identical in both specimens. As shown in Fig.13(c), they found no difference in fatigue limit of these two materials. Moreover, the fatigue limits of those two materials are in good agreement with the value predicted by Eq.(8). This result may be against conventional knowledge but was naturally predicted by *the $\sqrt{area}$ parameter model*.

INFLUENCE OF SHAPE OF DEFECTS AND INCLUSIONS ON FATIGUE LIFE

Looking at the S-N curves for materials containing small cracks , holes and carbides (see Figs.5, 7 and 13(c)), we can find a common feature that a defect having a sharp corner such as crack causes *shorter fatigue life* than a defect having round shape *at the stress higher than fatigue limit*, though the fatigue limit for both defects still keeps the identical value for the identical value of $\sqrt{area}$. This feature may be illustrated as Fig.14.

The feature of Fig.14 must be considered when we estimate fatigue lives of materials containing small defects. So long as we predict fatigue limit, we can apply *the $\sqrt{area}$ parameter model*. However, when we need to predict fatigue lives under variable amplitude loading, the problem will become very complicated. The reasons for the difficulty of predicting fatigue lives may be listed as follows.

(1) The crack initiation life depends strongly on the shape of defects.
(2) The crack initiation life depends strongly on the size of defects.
(3) The scatter of defect size contained in materials causes the scatter of fatigue life and fatigue limit.
(4) The change in the threshold stress intensity factor range ΔK_{th} during crack growth influences the value of stress effective to crack growth.

Thus, simple assumptions of initial shape and size of defect always result large error in fatigue life prediction. In this sense, the fatigue life prediction model must be made very carefully.

QUALITY CONTROL OF MATERIALS BY INCLUSION RATING BASED ON STATISTICS OF EXTREME

The rating of defects and inclusions by *statistics of extreme* (7,14,15) is useful not only for predicting fatigue strength but also for the quality control of materials.

Figures 15 and 16 show some examples which are measured and applied in Japanese industries(18,19,22).

CONCLUSIONS

The essence of *the $\sqrt{area}$ parameter model* was explained for the prediction of fatigue strength of metallic materials containing small defects, small cracks, nonmetallic inclusions, pores in cast alloys and inhomogeneities such as carbides and eutectic silicon.

The rating of defects and inclusions by *statistics of extreme* was also introduced as a useful method to predict the scatter of fatigue strength and as a quality control of materials.

REFERENCES

(1) Frost, N. E., *Proc. Inst. Mech. Eng.*, Vol.173, 1959, pp.811-835

(2) Kitagawa, H. and Takahashi, S., *Proc. 2nd Int. Conf. Mech. Behavior Mater.*, Boston, 1976, pp.627-631.

(3) Murakami, Y. and Endo, M., *The Behaviour of Short Fatigue Cracks*, EGF Publ.1, Edited by K. J. Miller and E. R. de los Rios, Mech. Engng. Publ., London, 1986, pp.275-293.

(4) Murakami, Y., Uemura, U., Natsume, Y. and Miyakawa, S., *Trans. Japan Soc. Mech. Eng.*, Ser. A, Vol.56, No.252, 1990, pp.1074-1081.

(5) Murakami, Y. and Endo, T., *Int. J. Fatigue*, Vol.2, 1980, pp.23-30.

(6) Murakami, Y., *Engng. Fract. Mech.*, Vol.22, 1985, pp.101-114.

(7) Murakami, Y., *Metal Fatigue: Effects of Small Defects and Nonmetallic Inclusions*, Yokendo Ltd., Tokyo, 1993, and Murakami, Y. and Endo, M., *Proc. Conf. Theoretical Concepts and Numerical Analysis of Fatigue*, Univ. Birmingham, EMAS, U.K., 1992, pp.51-71.

(8) Toriyama, T. and Murakami, Y., *J. Soc. Mater. Sci., Japan*, Vol.42, No.481, 1993, pp.1160-1166.

(9) Murakami, Y., Toriyama, T, Koyasu, Y. and Nishida, S., *J. Iron and Steel Inst. Japan*, Vol.79, No.6, 1993, pp.678-684

(10) Murakami, Y., Kodama, S. and Konuma, S., *Int. J. Fatigue*, Vol.11, No.5, 1989, pp.291-298.

(11) Duckworth, W. E. and Ineson, E., *Clean Steel, Iron Steel Inst., Sp. Rep.*, Vol.77, 1963, pp.87-103.

(12) Murakami, Y., Kawakami, K. and Duckworth W. E., *Int. J. Fatigue*, Vol.13, No.6, 1991, pp.489-499.

(13) Murakami, Y. and Usuki, H., *Int. J. Fatigue*, Vol.11, No.5, 1989, pp.299-307.

(14) Murakami, Y., Toriyama, T. and Coudert, E. M., *J. Testing and Evaluation*, Vol.22. No.4. 1994, pp.318-326.

(15) Murakami, Y., *J. Res. Natl. Inst. Stand. Technol.*, Vol.99, No.4, 1994, pp.345-351

(16) Gumbel, E. J., *Statistics of Extremes*, Columbia University Press, New York, 1957.

(17) Endo, M., *J. Soc. Mater. Sci., Japan*, Vol.38, No.433, 1989, pp.1139-1144.

(18) Sugiyama, Y., Asami, K. and Matsuoka, S., *69th JSME Spring Ann. Meeting*, Vol.A, No.920-17, 1992, pp.476-478.

(19) Kobayashi, M. and Matsui, T., *Trans. Japan Soc. Mech. Eng.*, Ser. A, Vol.62, No.594, 1996, pp.341-346.

(20) Murakami, Y., Ikeda, H. and Toriyama, T., *ICM6*, 1991, pp.433-438.

(21) Natsume, Y., Muramatsu, T. and Miyamoto, T, *Proc. JSME Meeting*, No.900-86, 1990, pp.323-325, and *private communication*.

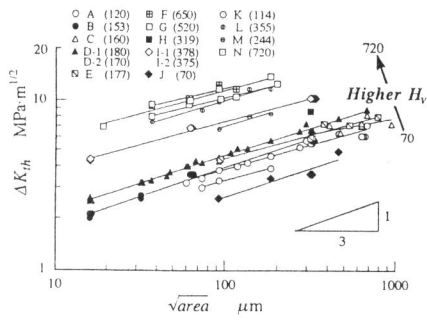(22) Ikeda, H., *Private communication* (Toyoda Automatic Loom Works).

Figure 1 Relationship between ΔK_{th} and $\sqrt{area}$ for various defects and cracks. Letters correspond to the materials given in reference (3). Numbers in parentheses indicate the Vickers hardness HV of materials.
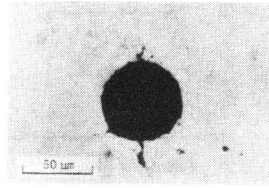
Figure 2 Nonpropagating cracks observed at fatigue limit of maraging steel ($HV = 740$) (4). $\sigma_w = 666$ MPa, $\sigma_m = -255$ MPa, Hole diameter = 50 μm, Hole depth = 70 μm.
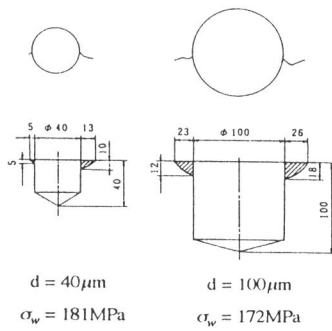

Figure 3 Interior shapes and configurations of nonpropagating cracks. 0.13% carbon steel (5).
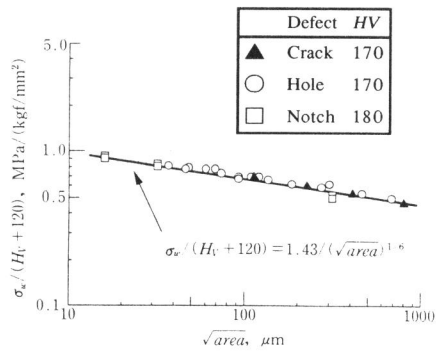
Figure 4 Relationship between $\sigma_w/(HV+120)$ and $\sqrt{area}$ for annealed medium-carbon steel specimens containing a crack or small defect (7).

3 9
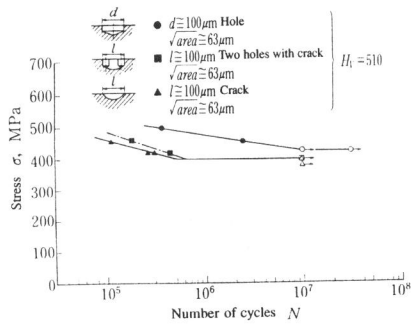
Figure 5 S-N curves for maraging steel having the hole and crack which have the same initial value of $\sqrt{area}$ (8).
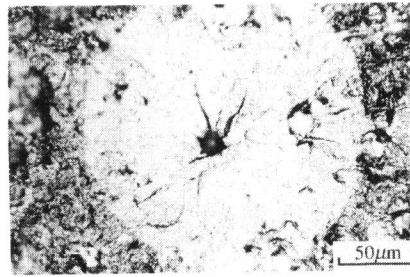
Figure 6 Typical example of fisheye. Rotating bending fatigue. $HV = 641$, $\sigma = 980$ MPa, $N_f = 1.69 \times 10^6$, $\sqrt{area} = 17.9$ μm, Distance from surface = 138μm. Chemical composition : Al-Ca-Mg-O (9).
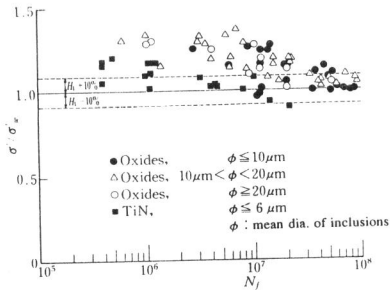
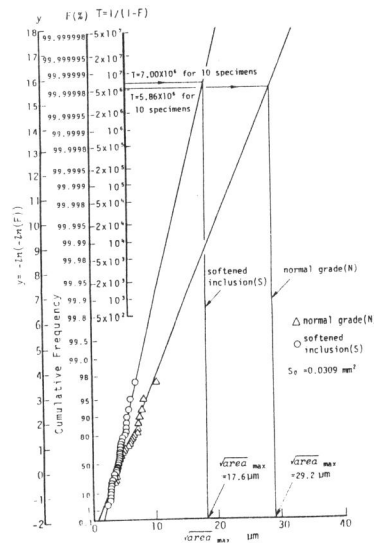Figure 7 Comparison between the failure stress σ' and the predicted fatigue strength σ'_w (Rotating bending fatigue. Bearing steel) (7).

Figure 8 Cumulative frequency of the extreme values of inclusions of spring steel (9). S_0 : Standard inspection area.
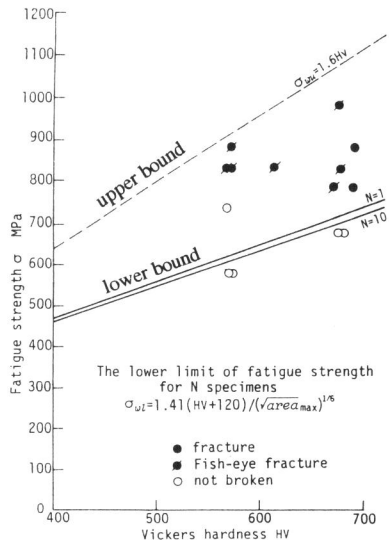
Figure 9 Comparison of the predicted lower limit of fatigue strength with the experimental results (Specimens with softened inclusions of spring steel) (9).
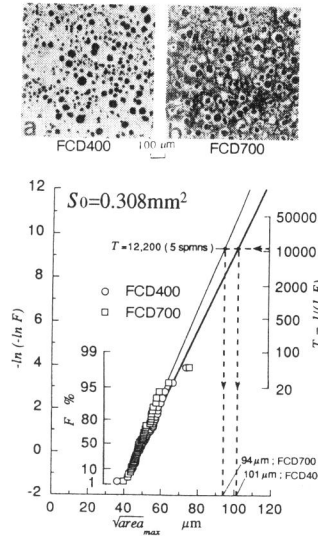
Figure 10 Distribution of maximum sizes of graphite nodules, $\sqrt{area}_{max}$, for two nodular cast irons (17). S_0 : Standard inspection area.
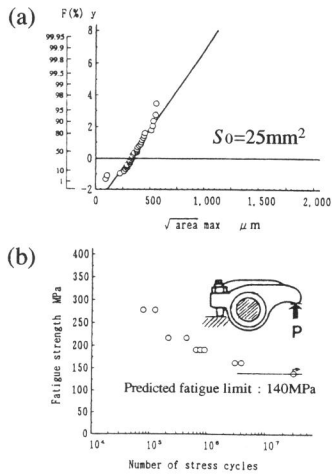

Figure 11 Al rocher arm of automobile (19).   (a)Distribution of extreme values for pore size.   (b)S-N curve.
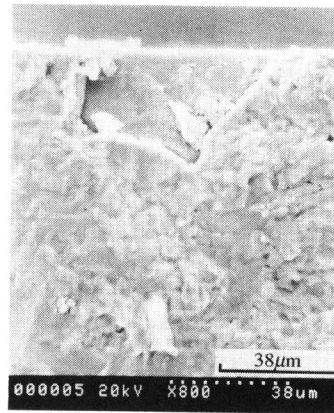

Figure 12 Fracture origin at Si-phase of an extruded Al alloy, High cycle fatigue test, σ= 196 MPa, N_f = 7 × 10⁶.
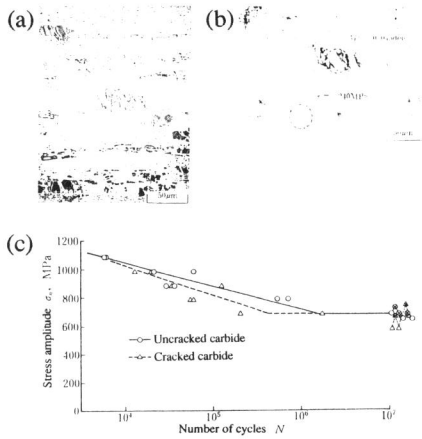
(a)

(b)

(c)

Figure 13 SKD-11 (Tool steel) (a) Uncracked carbides in microstructure. (b)Cracked carbides in microstructure. (c)S-N curve of tension-compression fatigue test for tool steel containing cracked or uncracked carbide (21).
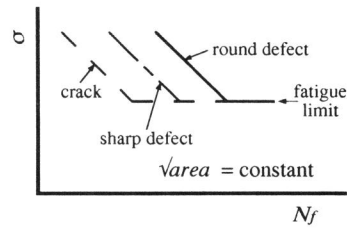
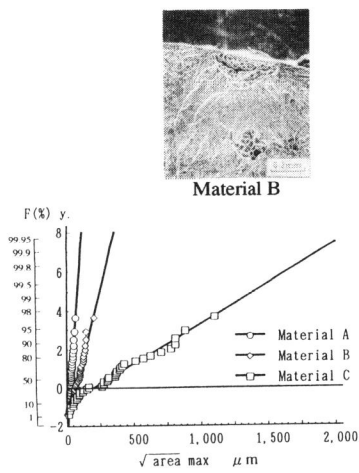Figure 14 Typical S-N curves for various defects having the same initial value of $\sqrt{area}$.

(a)

(b)

Material B

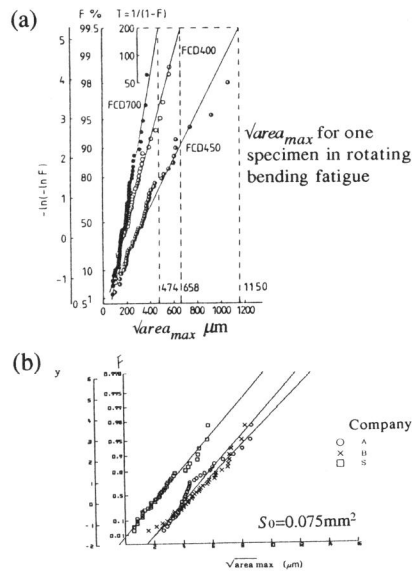Figure 15 Distribution of extreme values of pore size for 3 Al cast alloys (19). $S_0 = 44.16mm^2$ (Standard inspection area)

Figure 16 (a)Distribution of maximum sizes of defects, $\sqrt{area}_{max}$, for 3 nodular cast irons (18). (b) Distribution of maximum sizes of defects, for 3 flapper valve stainless steels (22).